On the improvement of the ductile removal ability of brittle KDP crystal via temperature effect

Qi Liu[1,2], Mingjun Chen[1], Zhirong Liao[2*], Junyuan Feng[3], Dongdong Xu[2,4], Jian Cheng[1*]

[1] Center of precision engineering, Harbin Institute of Technology, Harbin 150001, China

[2] Machining and Condition Monitoring Group, Faculty of Engineering, University of Nottingham, NG7 2RD, UK

[3] School of Mechanical Engineering, South China University of Technology, Guangzhou, 510640, China

[4] School of Mechanical Engineering, Tongji University, 201804, China

Abstract

Brittle KH_2PO_4 (KDP) crystal is difficult-to-machine because of its low fracture resistance whereby brittle cracks can be easily introduced in machining processes. To achieve ductile machining without any cracks, this type of materials is generally processed by some ultra-precision machining techniques at ambient temperature with nanoscale material removal, yielding low machining efficiency and high processing cost. Recently, thermal-assisted techniques have been used to successfully facilitate the machining of some difficult-to-machine materials, like superalloys, but little effort has been made to explore whether the temperature effect can contribute to the ductile machinability of brittle materials yet. Thus, the aim of this study is to figure out the specific role of temperature in the deformation behaviours of brittle KDP crystal by nano indentation/scratch methods. It is found that compared with those at ambient temperature (AT, i.e. 23 ℃), the hardness and Elastic modulus of KDP crystal at elevated temperature (ET, i.e. 160 ℃) decrease substantially by 21.4% and 32.5%, respectively, while the fracture toughness increases greatly by 15.5%, implying a higher ability of ductile deformation at ET. Meanwhile, the scratch length within ductile removal has been identified to be extended more than 4 times by increasing temperature from AT to ET. Both the quantity and size of brittle features (e.g., cracks and chunk removal) show a reducing trend with the increase of temperature. To uncover the underlying mechanism of this phenomenon, an updated stress field model is proposed to analyze the scratch-induced stress distribution by considering the evolution of material property at various temperature. These presented results are significant for the future design of specific thermal-assisted processing techniques for machining brittle materials efficiently.

Keywords: brittle materials, temperature effect, nano scratch, stress analysis, ductile deformation.

Corresponding author:

Email: Zhirong.Liao@nottingham.ac.uk (Zhirong. Liao); cheng.826@hit.edu.cn (Jian Cheng)

1. Introduction

Brittle potassium dihydrogen phosphate (KH_2PO_4/KDP) crystal, due to its extraordinary nonlinear optical performance [1], has been widely employed in laser-driven Inertial Confinement Fusion (ICF) facilities [2]. While in the practical working environment with intensely laser irradiation, it is extremely vulnerable to generate laser-induced damage defects (i.e., micro-cracks) on the surfaces of KDP optics, which severely restrict the output energy promotion and the stable running of ICF facilities [3, 4]. With the aim of recycling the use of these expensive KDP optics, the most economical and feasible approach is to repair the damaged optical elements as soon as any defect takes place [3, 5]. Nowadays, the micro ball-end milling technique has been accepted as the most potential solution to achieve the recycle loop of KDP optical components. Nevertheless, fabricating a crack-free repair surface on this type of optics still is a challenging task owing to the low harness [6], poor fracture resistance [7] and random crystallographic orientation of KDP crystal [7, 8].

In order to acquire a crack-free repair contour on the KDP surface, the damaged materials due to the laser irradiation are supposed to be repaired in ductile-regime whereby the critical undeformed cutting thickness (UCT) is normally identified as around hundreds of nanometers [3, 9]. This submicron-volume material removal means that not only an ultra-precision machine tool is required but a low machining efficiency is inevitable caused, ultimately increasing the fabrication cost of KDP optics. Thus, the values of UCT play a significant influence on the machining of brittle materials [3]. As known in the ductile machining theory [10, 11], the critical value of UCT for ductile cutting is highly dependent on the mechanical properties of targeted material, like hardness and fracture toughness [12, 13], but these mechanical characteristics of one material are highly related to its working temperature [14, 15]. Thus, interesting questions are proposed but not answered satisfactorily: does the temperature have an appealing effect on ductile deformation behaviours of brittle KDP crystal? Moreover, can this temperature effect be employed to benefit the ductile machining capacity of KDP? will this concept further enlighten the development of a new innovative cutting mechanism or technique to enhance the machining quality of other brittle materials?

For answering these questions, the first step is to understand the material property of KH_2PO_4 crystal. The cell of KH_2PO_4 crystal is generally indexed as a tetragonal crystallographic structure with a space group of $I42^d$ whereby the ionic bond connecting $[PO_4]^{3-}$ units and cations is one of the main factors causing the fragile property of this material [2]. Except for the brittle property, KDP crystal is much softer than other conventional optical materials (e.g., glasses[16], and polycrystal ZnSe [17]). The Mohs hardness of KDP is only 2.5, less than that of silver (3.0), causing great obstacles in its ultra-precision grinding processes because the grinding abrasives could get embedded into and damage machined surfaces. Meanwhile, for understanding the mechanical response of KDP crystal, a great

number of nano indentation tests were conducted with different indentation loads, which play a similar role to cutting forces in actual machining processes[18-20]. The results show that there are two slip groups in KDP [18]: one group consists of (101), (112), (123) and (110) crystalline planes with a vector of 1/2<111> while the other group is (010) <100>, giving brittle KDP crystal high flexibility to undergo plastic deformation which can be observed in the indentation load-depth curves with sudden depth bursts (~ 8nm) [19], named as pop-in event. However, these events have been identified to happen only at quite small indentation loads (several mNs). Once the applied loads increase to dozens of mNs, brittle cracks will take place [9, 21]. This scenario indicates that although plastic deformation can be achieved for KDP crystal at a low load range, brittle-regime material removal (e.g., cracks) would inevitably occur in actual micro-milling repair processes of KDP crystal as the observed milling forces is generally around 100 mN [9]. Besides, Yang and Zhang have revealed the deformation behaviours of KDP under complex stressings via molecular dynamics (MD) simulation, which can provide insights for uncovering the material removal mechanism of KDP crystal at the atomic scale [22]. Recently, interesting work has been reported by Huang [23] that the temperature could positively enhance the fracture resistance of z-cut KDP crystal in three-point-bend loading tests from 0.68 $MPa \cdot m^{1/2}$ at 23℃ to more than 1.0 $MPa \cdot m^{1/2}$ at 160℃. However, the detailed role of temperature in the comprehensive material property of KDP crystal and the related machinability is still uncovered.

The machinability of one material can not only be evaluated by its material properties estimated by nanoindentation tests but also be reflected by the material removal behaviours in nano scratch processes [24-26], which are normally employed to simulate the cutting behaviours in actual machining processes [27]. During nano scratch processes, different deformation morphologies arising on the residual scratch grooves provide essential information revealing the various removal behaviours of tested materials. For KDP crystal, the material removal behaviours at the micron-scale scratch depth are mainly through brittle failure (i.e., radial cracks, lateral cracks, edge-chipping) at ambient temperature [7]. The ductile-regime removal can only be observed within a small scratch depth (around hundreds of nanometers) at ambient temperature, accompanied by a smooth scratch groove. On the whole, it can be seen that the previous work has achieved great progress in understanding the mechanical response of brittle materials to nano-indentation loads [19, 28] and in identifying the corresponding material deformation behaviours in nano scratching processes [14]. However, very little effort has been made to reveal how the temperature affects the change of material characteristics as well as various material removal behaviours.

Recently, we have attempted to answer this question by conducting nano scratch techniques on KDP crystal [21]. It is revealed experimentally that the critical UCT of brittle-to-ductile transition increases generally as the temperature rises from 23 ℃ to 180 ℃ and achieves its maximum value at

around 160 ℃~170 ℃. The critical UCT at 170 ℃ (~3.61μm) could be improved more than 8 times from that at 23 ℃ (~0.4μm). Nevertheless, there is still no systematical theoretical analysis and modelling work to explain these interesting experimental phenomena. Normally, the specific deformation behaviours developed in scratch progress can be explained by the stress analytical models proposed by Yoffe [29]and Ahn [30]. However, the influence of temperature on the instantaneous stress distribution during scratch processes and also the resultant material removal behaviours is not considered in these existing literature [29, 30]; and thus, further refinement of these aforementioned models is in need to analyze the scratch processes when considering the temperature effect.

For bridging this gap, this study aims to reveal the specific role of temperature in the ductile machinability of brittle KDP crystal by nano indenter techniques. To achieve this, the specific evolution of material properties induced by temperature change was firstly recalled briefly, followed by varied-depth scratch tests for revealing material removal behaviours at both ambient and elevated temperature. Especially, an analysis model is proposed to understand the residual stress field for figuring out the specific stress components regarding various deformation behaviours by taking into consideration of temperature effect. This presented work can contribute to the development of advanced thermal-assisted setups/methods for machining this type of brittle materials.

2. Nano indentation/scratch experiment design considering the temperature effect

As illustrated in Fig. 1, the nano-indentation and nano-scratch tests were carried on a nano-indenter (Nano Test, UK), which can achieve the testing temperature ranging from ambient temperature to 750°C . In this work, all the nano-indentation and nano-scratch tests were conducted at both ambient temperature (AT, i.e. 23°C) and elevated temperature(ET, i.e. 160°C), as it was reported that the fracture resistance of KDP increases as the temperature rises and peaks at 160°C [23]. During the tests, the elevated temperature can be achieved by heating the indenter platform (heating rate: 1°C/min), where the KDP samples were glued on, with a 30 min holding period at the designated temperature for stable thermal equilibrium. The used KDP specimen was polished in advance to eliminate any subsurface damage generated in previous processing and the adopted crystal plane in this work belongs to typical Double-Plane, the crystallographic structure of which is shown in Fig. 1(b). A spherical diamond indenter with a cone angle of θ=60°was employed for the nano tests, the radius of which is about 2.436 um (see in Fig. 1c). The reason for adopting spherical indenters rather than Berkovich and Vikers indenters which are common in nanoindentation experiments [7, 14] is that both the geometrical shape and size of spherical indenters are similar with those of the cutting edge of micro ball-end milling cutters used in the repair process of the surface defects on KDP optics [31, 32].

The nano-indentation tests were conducted to acquire the evolution of the material property of KDP (e.g., hardness (*H*), elastic modulus (*E*), and fracture toughness (K_{IC})) induced by the temperature effect. All the indentation trials were conducted at load-control mode with different maximum loads ranging from 10 ~50 mN (in a step of 10 mN). A 20 s holding time was set at the designated load P_{max} at the end of the loading stage, followed by an unloading stage. Each test is repeated three times. While the scratch tests were performed in the varied-depth mode at AT and ET, respectively, to get an insight into the brittle-to-ductile behaviours of KDP crystal. The applied normal scratch load was increasing from 0 mN to 150 mN while the scratch length was set as 450 um. As illustrated in Fig. 1b, all the scratches were performed perpendicular to the [110] direction on the Double plane as this orientation has the largest capability to achieve ductile cutting on this specific plane. More information about these nano tests can be found in our previous work [21]. Finally, an SEM instrument (JEOL 7100) was employed to observe surface morphologies generated in the above nano tests.

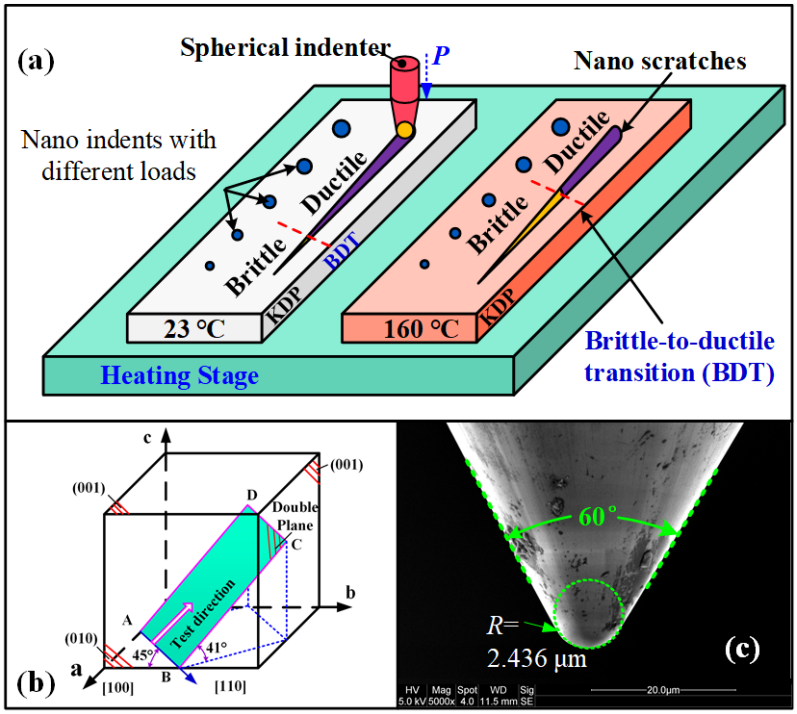

Fig. 1 (a) Schematic illustrating the nano indentation and scratch test at different temperatures; (b) The Double-Plane of KDP crystal used for the nano tests; (c) The spherical indenter tip used for nano tests.

3. Influence of temperature on material properties of KDP crystal revealed by nano-indentation test

As aforementioned, temperature plays a significant role in material properties and ultimate machinability. Thus, in this section, the particular material response of KDP crystal (e.g. *H*, *E*, K_{IC}) to nano indentation loads at different temperature will be discussed comprehensively.

3. 1 Nano indentation features developed at different temperatures

The indentation load-displacement curves are of great significance to reveal the material deformation and response behaviours to various indentation conditions. Fig. 2 shows the load-displacement curves obtained from the nano indentation of KDP crystal at different loads and temperatures. It can be seen that at the loading stage, the indentation displacements increase with the rise of applied loads at both AT and ET. However, at the unloading stage, the slope of initial unloading curves at ET turns negative, which is contrary to that at AT indentations. These negative slopes imply that a viscoelastic recovery behaviour took place in the unloading stage of ET indentations rather than the elastic recovery that occurred in AT indentation processes. Since the viscoelastic deformation is a combined behaviour of elastic and viscous deformations [33], this viscoelastic phenomenon that occurred in ET indentations should be attributed to the viscous deformation due to the thermal activation. But it is worthy to point out that this viscoelastic behaviour for KDP crystal is not only temperature-dependent but also load-independent as it was absent in the ET indentation curves with a small maximum load (P_{max}=10 mN).

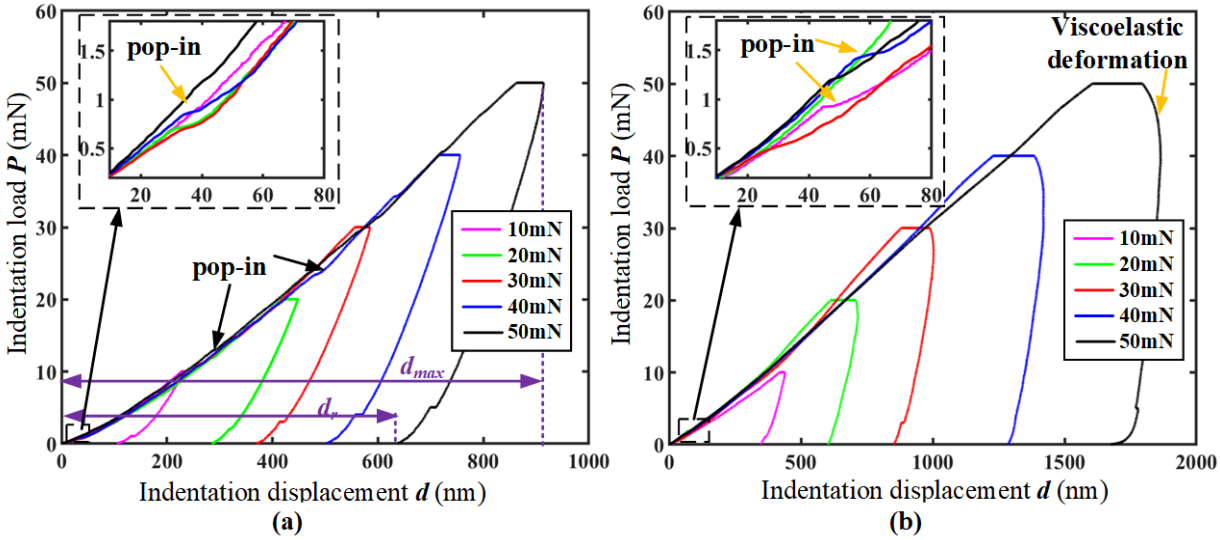

Fig. 2 The indentation load-displacement curves under various indentation loads: at ambient temperature (a); at elevated temperature (b).

Meanwhile, it is found that many pop-in events (i.e. abrupt drifts of indentation displacement) took place during the loading stage. When at small indentation loads (P<1.5 mN), the pop-in events tend to take place at both AT and ET (shown in the enlarged images in Fig. 2). While at large indentation load (dozens of mNs), the pop-in events occur frequently at AT with obvious displacement drifts (marked by black arrows in Fig. 2a) but can not be clear recognized at ET. It worthy to note that the pop-in events may have different generation mechanism. The pop-in events occurred at small indenation loads should be attributed to the plastic deformation caused by slipping as reported in Ref [34], while at large indentation loads, the pop-in events with obvious displacement drifts at AT (marked

by black arrows in Fig. 2a) may be induced by the sudden formation of cracks during the indentations. Moreover, the absence of pop-in events (i.e., cracks) at large loads in Fig. 2b further indicate the ductility improvement of KDP crystal at ET due to the thermal-activated plastic deformation. During the ET nano indentation processes, increasing the temperature could contribute to the improvement of atomic mobility and also the reduction of minimum stresses which are prerequisites for the nucleation of dislocations [10, 35]. Therefore, under this increasing stress field concerning the increasing indentation load, the dislocations are extremely easy to form, ultimately contributing to the formation of thermal-activated slip and plastic deformation.

The specific influence of temperature on the material response behaviour can also be proved by the surface morphologies of indentation impression. Fig. 3 shows the residual morphologies of KDP monocrystal developed at AT and ET with a maximum indentation load of 50 mN. Similar to previous experimental observation [21], one can see that in addition to some radial cracks, a great number of micro debris occurred on the residual surfaces indented at AT, as shown in Fig. 3(a), implying a very brittle crack behaviour engaged into the indentation process. While at ET, it is interesting to find that the plastic deformation dominated the indentation process although a few micro cracks developed at the indentation borders. This phenomena regarding the different surface morphologies at AT and ET clarify that increasing temperature exerts a positive role in enhancing the plastic deformation capacity of brittle KDP crystal.

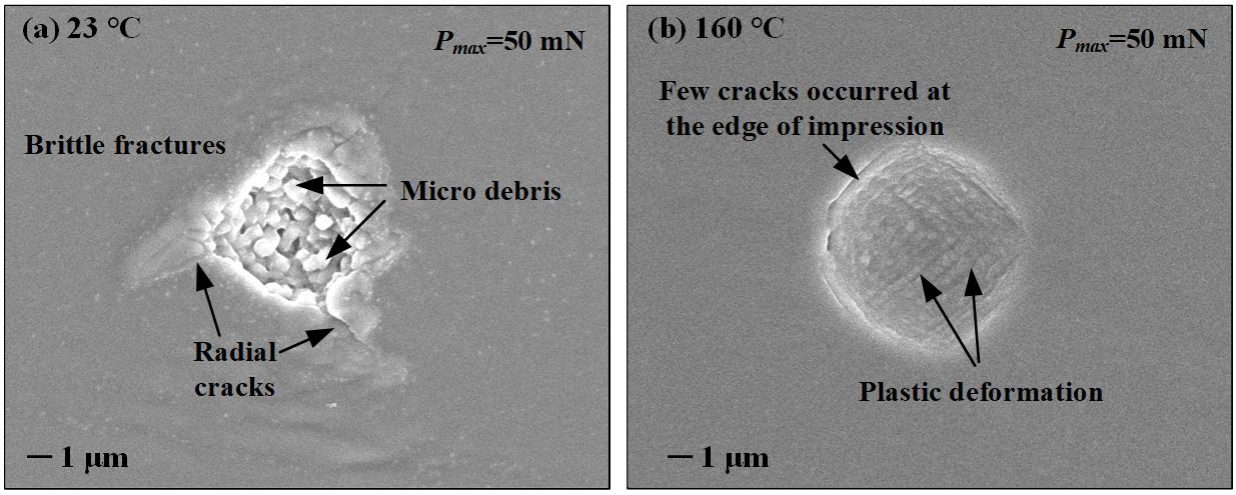

Fig. 3 The residual impression morphologies of spherical indentation (P_{max}=50mN) at different temperatures: (a) at ambient temperature; (b) at elevated temperature. Similar observations have also been achieved in [21].

3. 2 The evolution of material properties induced by temperature effect

To further understand the role of temperature in the material deformation behaviours, the mechanical characteristics of KDP (e.g. H, E, K_{IC} and recovery rate) at AT and ET will be calculated and discussed comprehensively based on the nano-indentation results. During the unloading process,

the deformed materials underneath the indenter will recover with the leave of the indenter tip. In this work, the recovery rate is defined as $\zeta=\frac{d_{\max}-d_r}{d_{\max}}\times 100\%$, where the $d_{\max}$ and d_r are the penetration depth and residual depth in the indentation process, respectively. The evolution of these three indexes (i.e., $d_{\max}$, d_r, and ζ) with the increase of applied indentation loads at these two temperatures are depicted in Fig. 4. One can see that at both AT and ET, the $d_{\max}$ and d_r all witness a growing trend with the rise of applied loads while the recovery rate firstly reduces substantially at a small load range (<10 mN) and then becomes prone to be stable at a high load range. Nevertheless, it is worthy to note that the recovery rate at ET is much lower than that at AT. Especially at the high load range, the ζ at ET is only around 10% while that at AT is more than 30%, indicating that the recovery deformation capacity at ET decreases dramatically compared with that at AT. The overall reduction of recovery rate at ET illustrated the energy consumption used for plastic deformation during indentation at ET could be higher than that at AT with each applied load considering the energy conservation.

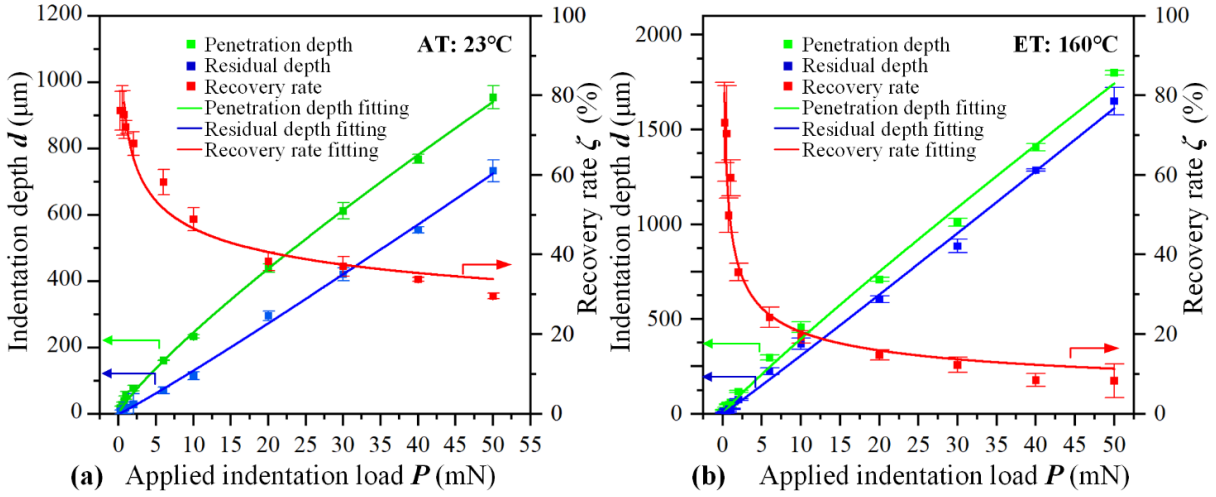

Fig. 4 The relationships between the applied indentation loads and penetration depth, residual depth and recovery rate at different temperature : (a) at ambient temperature; (b) at elevated temperature.

Moreover, the specific mechanical characteristics (e.g. H, E, K_{IC}) of KDP crystal at AT and ET were estimated based on the Oliver-Pharr's approach [36] and fracture mechanic theory [37] (see in Appendix. A), to gain insight into the specific effect of temperature on its ultimate material removal behaviour during machining and the resultant surface integrity. Fig. 5 shows the measured material properties of KDP crystal in the case of nano indentation with P_{max} =10mN at both AT and ET. The measured values at ambient temperature are consistent well with the reported values (H=2.0±0.2 GPa, E=38.7 Gpa, K_{IC}=0.24 Mpa·m$^{1/2}$) in the literature [38, 39], indicating the accuracy and reasonability

of the measurement. Compared with the estimated values at AT, the H and E of KDP crystal at ET decrease to 1.54±0.11 GPa by 21.4% and 24.10±0.75 GPa, by 32.5%, respectively, while the fracture toughness increases to 0.2856±0.0041 Mpa·m$^{1/2}$ by 15.5%. Both the decrease of H and E and the increase of K_{IC} jointly demonstrate the increased flexibility of ductile deformation of KDP crystal at ET. The atoms inside materials and their related motion at ET could become more intensive due to the increased temperature, giving the rise to the reduction of the attraction forces between adjacent atoms [10]. Given the increased indentation load, these affected atoms are, consequently, much easier to run away from their balance positions, contributing to the generation of dislocations due to the thermal activation effect.

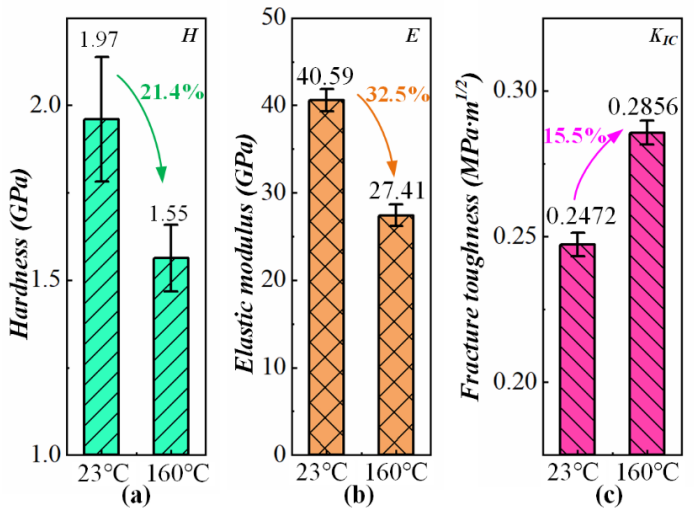

Fig. 5 The measured material mechanical characteristics of KDP crystal at ambient and elevated temperature: (a) hardness (H); (b) elastic modulus (E); (c) fracture toughness (K_{IC})

4. Understanding the material machinability behaviours induced by the temperature effect

The results presented in Section 3 clear illustrate that raising temperature indeed has an interesting influence on the machineability of KDP by affecting the material properties. Thus, to further reveal the specific effect of temperature on material cutting behaviors of KDP, the detailed material removal behaviours during nanoscratch processes and the related formation mechanism will be discussed in this section.

4.1 Comparison of material removal behaviour during the scratch process of KDP crystal at AT and ET

The residual morphology features on the scratch grooves are beneficial for understanding different material removal behaviours, especially for difficult-to-machine materials [14, 40]. The specific material removal behaviours at AT and ET have been discussed in our previous work as

aforementioned [21], but in order to help the potential readers better understand the foregoing theoretical stress analysis, the corresponding SEM images of varied-depth scratch morphologies at AT (i.e. 23°C) and ET (i.e. 160°C) will be introduced briefly in this work and are presented in Fig. 6 and Fig. 7, respectively. One can see that, with the increase of applied loads (see in Fig. 6), many brittle features are prone to occur on the groove surfaces, indicating that the brittle mode is gradually dominating in the material removal process as the scratch load increases. More specifically (see in Fig. 6a), the ductile removal can only be achieved at the beginning stage with a short distance (< 32 micrometers). But typical brittle features (e.g. radial cracks and micro pits) come into being on the residual groove (see in Fig. 6ii) with the rise of applied load, The included angle between these radial cracks and scratch direction is about 45°, which indicates that the maximum stress direction as the brittle cracks has been identified to propagate along the direction of maximum stress [40]. Meanwhile, the magnified image in Fig. 6(iv) (detail of zone Fig. 6ii) clearly show there are a great number of micro debris left on the residual grooves, which look like those taking place on indentation surfaces at AT (see Fig. 3a) and further proof the brittle removal behaviours. As the scratch load increases further, many transverse cracks start to emerge on the scratch groove and tend to propagate to the surface of bulk material, giving the risk of the generation of edge-chippings.

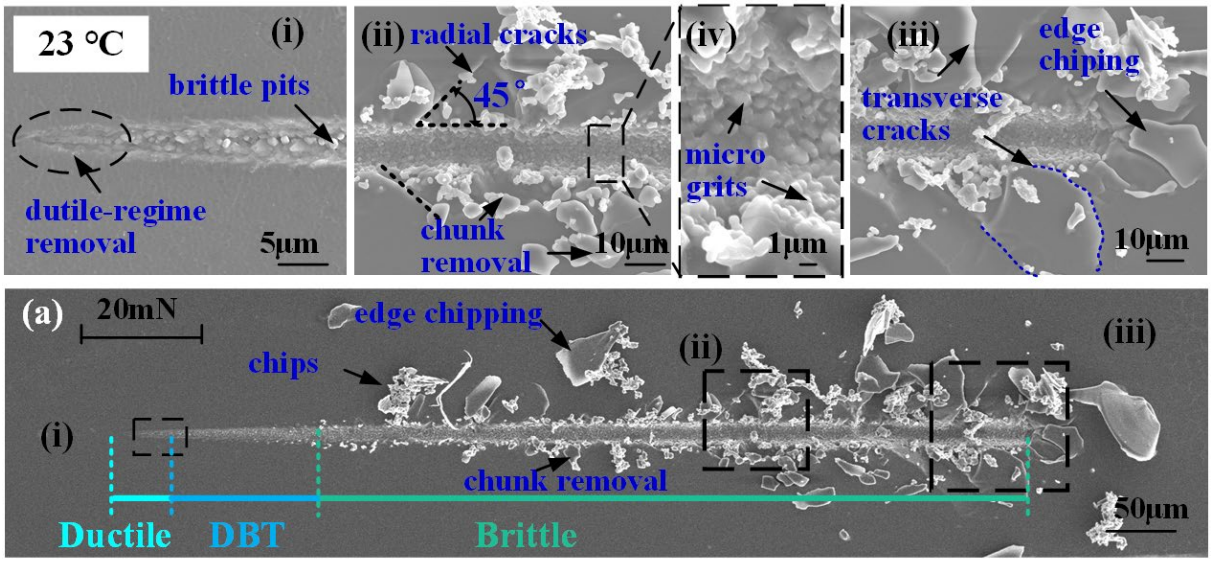

Fig. 6 Surface SEM images of the scratch at ambient temperature (23°C); The enlarged images (i-iv) showing representative material removal behaviours; Similar observations can be found in the previous experimental study [21].

Regarding the scratch grooves generated at ET, the surfaces morphologies are presented in Fig. 7. One can see that many ductile features are engaging in the material removal process at ET. Different to the short plastic groove length at AT, the scratch length of the smooth groove at the beginning stage increases by about 4 times (~141 μm), indicating a significant enhancement of the ductile removal capacity at ET. As the scratch load further rises, a few radial cracks start to take place on the residual

groove (see in Fig. 7ii), which is an obvious signal of brittle removal behaviours. At the high load range, both the quantity and size of the radial cracks display a rising trend with the continuing increase of scratch loads, as shown in Fig. 7(iii-iv). Meanwhile, there is some chunk removal occurring at the end of the scratch, which may be attributed to the crack propagation and interaction.

By comparing the scratch surface morphologies generated at AT and ET, it can be found that the most of brittle features (e.g., transverse cracks and edge chippings) at AT disappeared on the scratch grooves at ET whereby there are more ductile removal behaviours (i.e. smooth surface with a quite long scratch length). It is interesting to note that there is no residual debris observed at ET which differs from the observation at AT where the debris was formed even at the ductile scratch region (Fig. 6). Overall, the evolution of scratch surface morphologies induced by temperature keeps consistent with the indentation results presented in Section 3.1, collectively demonstrating that raising temperature could have a positive influence on the ductile removal of brittle materials, and also indicating that this temperature effect can be employed to enhance the machining quality and efficiency of KDP crystal by adopting large-value undercut chip thickness.

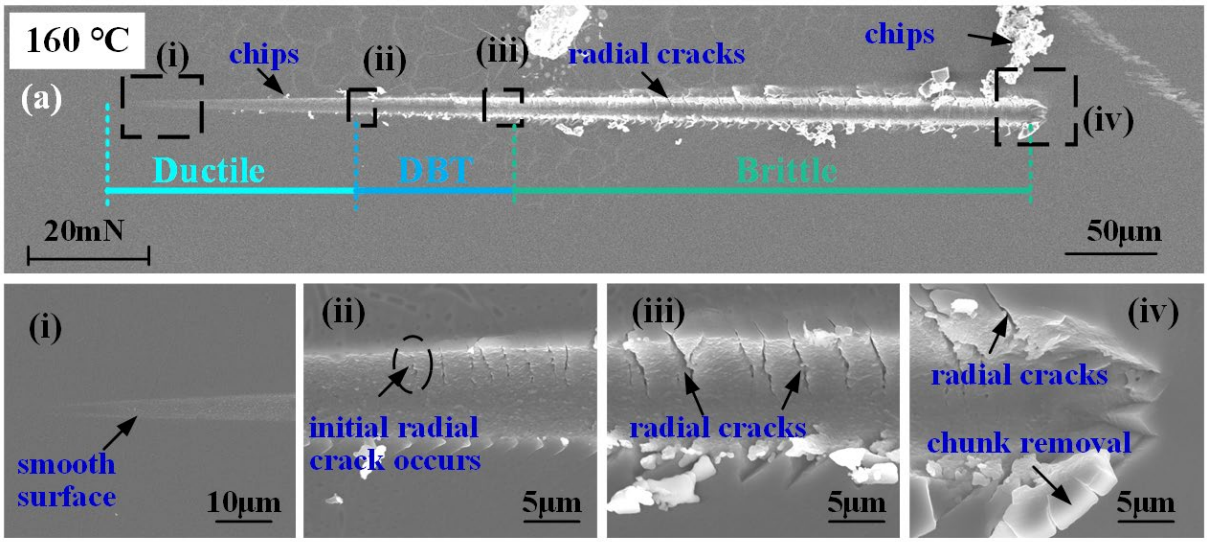

Fig. 7 Surface SEM images of the scratch at elevated temperature (160°C); The enlarged images (i-iv) showing representative material removal behaviours. Similar observations can be found in the previous experimental study [21].

4.2 Development of the stress models for understanding the stress distribution that occurred at different temperature

According to existing studies, both the plastic and brittle behaviours occurring in scratch processes have a close relationship with the stress distribution underneath the indenter tip [30]. Thus, it is necessary to understand the deformation behaviours, as observed above, developed in the varied-depth scratches at different temperature from the view of stress analysis.

It has been reported that the stress distribution responsible for brittle cracks consists of an elastic stress field and a residual stress field [41, 42]. The first one arises from the Boussinesq field induced by normal load, P_n, and the Cerruti field induced by tangential force, P_t, while the latter one derives from the Blister field due to residual stresses which are attributed to the local inelastic deformation generated in the scratch. Therefore, the overall scratch stress can be described as:

$$\sigma=\sigma^{n}_{Boussi}+\sigma^{t}_{Cerruti}+\sigma^{r}_{Blister} \quad (1)$$

$$\tau=\tau^{n}_{Boussi}+\tau^{t}_{Cerruti}+\tau^{r}_{Blister} \quad (2)$$

The specific equations for estimating each stress field can be found in the Appendix. B. Fig. 8 illustrates the schematic of scratch processes and the related coordinate system for describing stress components. It is worthy to note that the content shown in Fig. 8a is about the scratch process with a constant depth rather than the varied-depth scratch adopted in this work, but the presented schematic is reasonable to be used to describe the development details of the stress models regarding the varied-depth scratch process. This is because the detailed material deformation behaviours (i.e. material removal and recovery) and the related contact areas between the indenter tip and specimen (Fig. 8b and c) in varied-depth scratch process at one specific moment (i.e. with a specific scratch load) can be regarded similar to those developed in the constant-depth scratch process with the same scratch load. In this nano scratch test, except for the applied normal load (P_n,), the tangential load (P_t,) exerts a significant role in the stress distribution, especially in the Cerruti stress field. The generation of the tangential load is mainly due to the friction between the indenter tip and workpiece, which can be estimated by [43]

$$P_t=(\mu_{ploughing}+\mu_{interface})P_n \quad (3)$$

$$\mu_{ploughing}=A_t/A_n \quad (4)$$

where $\mu_{ploughing}$ and $\mu_{interface}$=0.3 are the ploughing friction coefficient and interface friction coefficient [43], respectively. A_t and A_n are normal-projected area and tangential-projected area of the tool and workpiece zone, respectively, and can be described as [44]:

$$A_n=\frac{1}{2}\pi(2Rh-h2)+\frac{4}{3}\sqrt{2Rh-h^2}\times\sqrt{2(R+h_f)-(2R+h_f^2+h^2)} \quad (5)$$

$$A_t=R^2\arccos(\frac{R-h}{R})-(R-h)\sqrt{h(2R-h)} \quad (6)$$

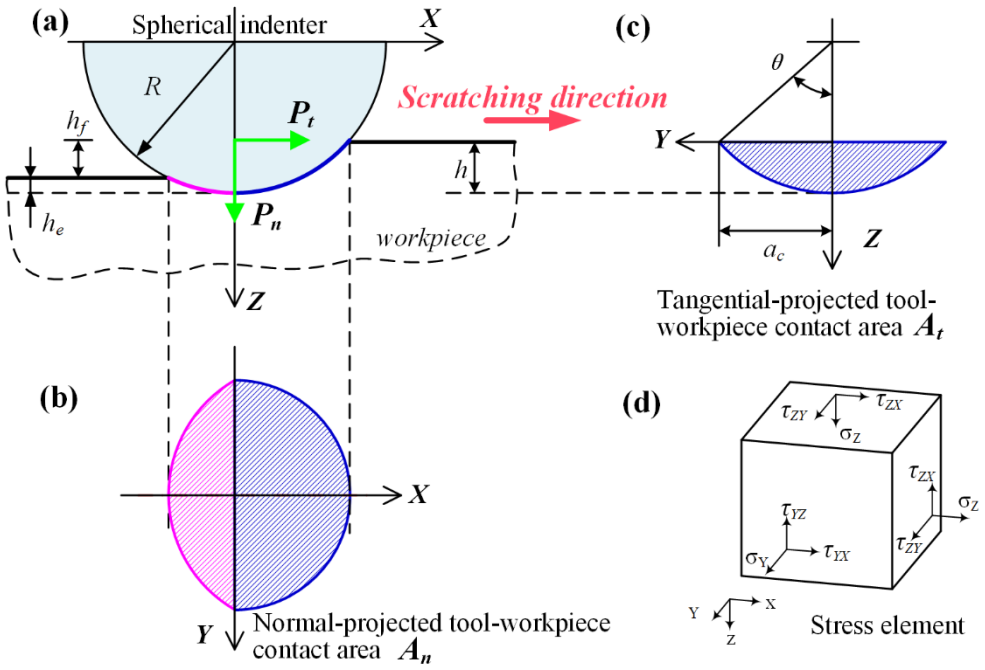

Fig. 8 Schematic of scratch processes with a spherical indenter tip (a); contact area between indenter and workpiece (b) (c); coordinate system of stress components (d).

The values of the projected area (A_t and A_n) in this work are highly related to the practical penetration depth (h), which can be referred to the scratch depth-load curves as shown in Fig. 9. By analyzing the smoothness extent of the depth-load curve, both the curves at AT and ET can be divided into three sections: smooth curves (ductile regime), curves start having a few flutters (BDT regimes), curves have severe fluctuations (brittle regime). These different curve sections can be linked with the various scratch morphologies shown in Fig. 6 and Fig. 7 as they are all the outcomes of material removal behaviours developed in the scratch process. Meanwhile, it is found that the depth-load curve at AT has a great number of severe fluctuations due to the generation of brittle fractures while that at ET tends to be more smooth, especially at the small scratch load range (see in the enlarged image in Fig. 9). This phenomenon further proves that the ductile removal ability of KDP crystal can be greatly enhanced by improving the temperature.

Meanwhile, as shown in Appendix. B (Eqs. B13-18), there is a key important factor, B, affecting the Blister stress distribution caused by the local inelastic deformation. This factor, B, is known as the Blister strength, and can be expressed as follow, according to Wang's analysis [41]:

$$B = f\frac{3Ea^2}{4\pi(1-2\nu)(1+\nu)}\cot\theta \tag{7}$$

where ν is the material poison's ratio while θ is the half-apex angle of indenters. f is a compaction factor that can be estimated as the ratio of elastic-deformation volume to the whole deformation volume

generated in indentation or scratch processes [17]. Thus, in the presented work, the compaction factor, f, can be simplified as the ratio of the recovery rate ζ, as discussed in Section 3.2：

$$f=\zeta=\frac{\left(d_{\max}-d_r\right)}{d_{\max}} \tag{8}$$

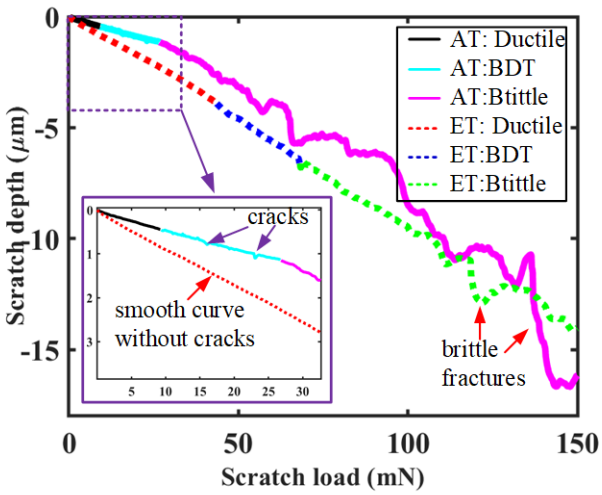

Fig. 9 The depth/load curves of scratch grooves generated at ambient temperature and elevated temperature.

Besides, according to indentation theory [36], the contact size a in Eq. (7) is highly related to the indentation load and hardness. Meanwhile, considering the analogy of indentation-to-scratch hardness, the contact size a can be described as:

$$a=\lambda\sqrt{P/(\pi H)} \tag{9}$$

where λ = 1 is a geometric factor in this case with a spherical axisymmetric tip [36].

Therefore, by substituting Eqs. (8-9) into Eq. 7, the Blister strength can ultimately be given by

$$B=P_{\mathrm{n}}\frac{E}{H}\frac{3\lambda^2\left(d_{\max}-d_r\right)}{4\pi\left(1-2\nu\right)\left(1+\nu\right)d_{\max}}\cot\theta \tag{10}$$

Given the obvious effect of temperature on the material response to indentation loads as in the Section 3, the temperature could also have an important influence on the Blister strength B by affecting the material properties (e.g., Elastic modulus, hardness and material elastic recovery rate), eventually exerting a significant role in the whole tress field underneath the scratch grooves and further the material deformation behaviours.

4.3 Stress distribution analysis for understanding the material removal behaviours at AT and ET

4.3.1 Comparison of the stress field on the cross-sectional plane at AT and ET

Based on the updated stress field models, the specific deformation behaviours occurred in the scratch process can be analysed. In this work, the discussion on the scratch-induced stress distribution underneath the scratch indenter tip is performed combining the scratch loads of 10mN and 50mN at both AT and ET. The reason for choosing these two specific scratch loads is that, based on the observation of scratch load/depth (*P/h*) curves (Fig. 9), the scratch zone with P_n=10mN at AT and P_n=50 mN at ET can be approximately considered as the turning points of the scratch changing from ductile-regime to brittle-regime as the scratch *P/h* curves seem to start to fluctuate due to crack generations under these two specific conditions. Meanwhile, the scratch area with P_n=50mN at AT is total brittle while that with P_n=10mN at ET is ductile, providing an obvious comparison for understanding the relationship between stress distribution and material deformation behaviours.

Besides, in order to better clarify the temperature effect, the stress is calculated accordingly in the form of normalized stress ($\sigma\pi\kappa c^2 / P_n$ [45]). The index κ and c are dimensionless constant and the corresponding scratch depth ($c = h$) under the scratch load P_n (see in Fig. 9), respectively. It is found that although the stress values at AT and ET are deeply affected by the temperature effect, the stress distribution patterns in these cases are similar. Thus, only the stress distribution at AT with P_n=50mN on the cross-sectional plane (YOZ) is presented in this study, as shown in Fig. 10, to illustrate the distribution patterns of different stress components. The stress components $\boldsymbol{\sigma_x}$, $\boldsymbol{\sigma_y}$ and $\boldsymbol{\sigma_z}$ have been identified to be responsible for the initiation of radial cracks, medial cracks and lateral cracks [41], respectively. In this case, the stress components $\boldsymbol{\sigma_x}$ and $\boldsymbol{\sigma_z}$ are found to reach their maximum tensile stress values underneath the indenter tip while the stress component $\boldsymbol{\sigma_y}$ has two tensile stress zones on both sides of the tip. The specific relationship between stress distribution patterns and crack initiation will be clarified with the foregoing discussion on the analysis of the stress field along the XOZ plane.

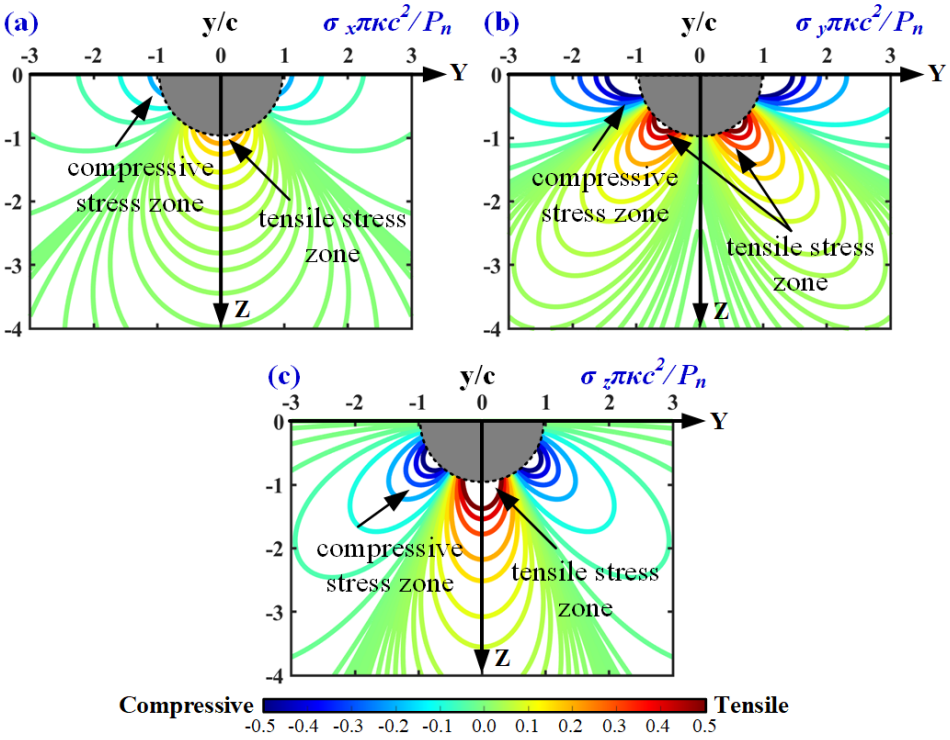

Fig. 10 The normalized stress distribution of different stress components at the position with a scratch load of P_n=50 mN at ambient temperature: (a) normalized stress of σ_x ; (b) normalized stress of σ_y ;(c) normalized stress of σ_z.

Here, the main objective is to explore whether the temperature has a positive influence on stress distributions and material deformation occurred in the scratch process. Fig. 11 shows the stress field distributed along the Y-axis direction at various scratch conditions. One can see that the temperature effect exerts a significant role in reducing the stress intensity underneath the indenter tip induced by scratching. The tensile stress values of all stress components at ET with P_n=10mN are found to be lower than those at AT, as shown in Fig. 11(a-c). This phenomenon might be attributed to the higher flexibility of material deformation induced by the thermal-activated dislocation as above discussed. Meanwhile, it is worthy to note that the difference in the tensile stress between AT and ET is prone to be larger as the scratch load increases. Referring to the Fracture Mechanic theory [3, 46], brittle cracks will occur only when the local stresses exceed the material fracture toughness. Thus, the low-value stress field at ET could highly reduce the possibility of crack initiation and propagation, eventually contributing to the material ductile-removal in actual machining processes.

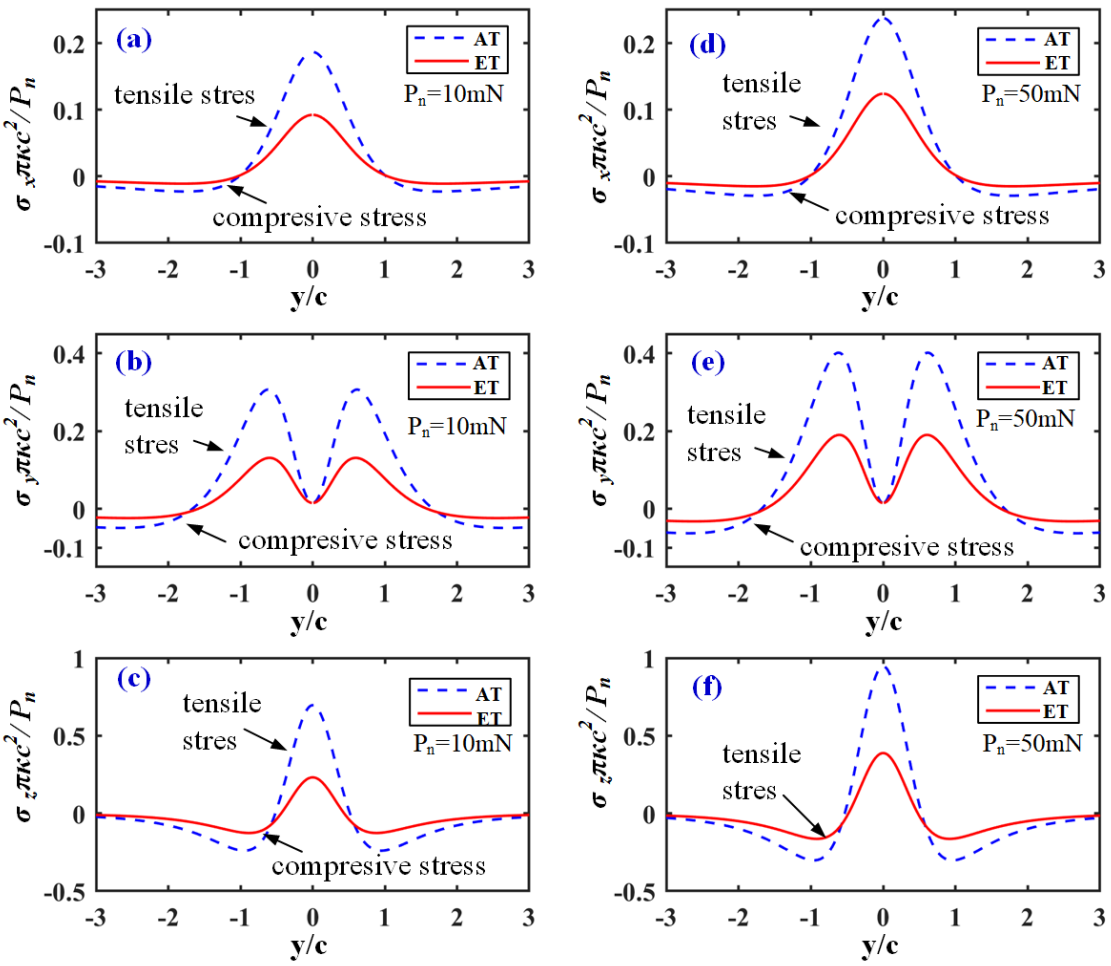

Fig. 11 Comparison of the stress distribution at the ambient temperature and elevated temperature at different normal loads: the normalized stress of σ_x at P_n=10 mN (a) and P_n=50 mN (b); the normalized stress of σ_y at P_n=10 mN (c) and P_n=50 mN (d); the normalized stress of σ_z at P_n=10 mN (e) and P_n=50 mN (f).

4.3.2 Comparison of the stress field along the scratching direction at AT and ET

The deformation behaviours developed in the scratch process are not only highly related to the stress distribution on the cross-sections plane (YOZ) but also deeply affected by the stress field parallel with the scratch direction. Thus, it is of great importance to analyze the stress field on XOZ plane for clarifying the deformation behaviours in-depth.

Fig. 12 shows the stress components, $\boldsymbol{\sigma_x}$, in the XOZ plane with a normal load of P_n=50 mN. It can be seen that in the area before the indenter, the stress component, $\boldsymbol{\sigma_x}$, maximizes at the elastic-plastic deformation interface with an included angle of φ=16.69° with the Z-axis (Fig. 12a). While the area behind the indenter tip undergoes the gradually unloading stage of the scratch load. This means that the elastic stress generated by the scratch load in this area would decrease quickly with the advance of the indenter tip. Consequently, the stress field in the rear of the tip would gradually transfer into Blister residual stress. Furthermore, the stress component in the rear of the tip is identified as tensile

stress, the contour line of which is almost parallel to the scratch direction. This tensile stress concentration condition gives a high risk of the formation of brittle radial and lateral cracks.

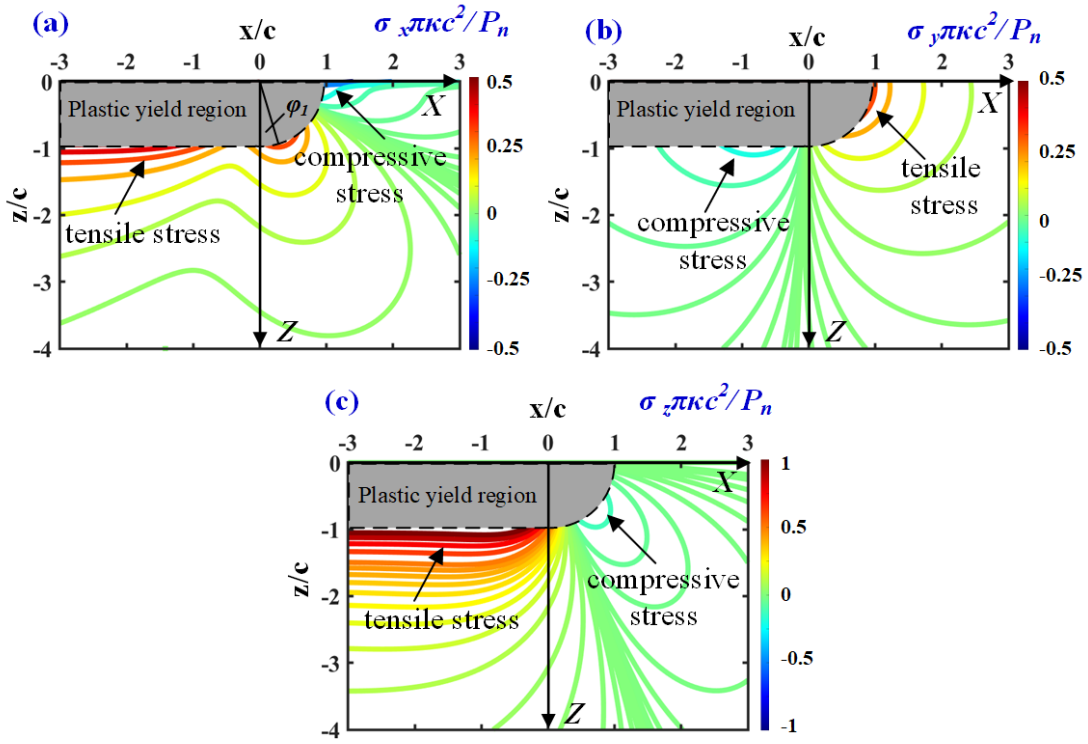

Fig. 12 The normalized stress distribution of different stress components in the XOZ plane at ambient temperature with the scratch load of P_n =50 mN: (a) normalized stress of σ_x ; (b) normalized stress of σ_y ;(c) normalized stress of σ_z.

Similarly, the stress component, $\boldsymbol{\sigma_y}$, comes to its peak value in the area before the indenter tip at the elastic-to-plastic deformation interface (Fig. 12b). This tensile stress is vertical to the scratch direction so that median cracks could be introduced. However, it is interesting to find that the maximum value of this tensile stress is quite small and seems to be lower than those shown in Fig. 12a and b. This should be attributed to the extrusion effect of the blunt spherical indenter tip, which could diverge the material in front of itself to both sides like a sharp Berkovich indenter tip [47]. Thus, although the stress in this area along Y-axis is tensile, the possibility of median crack initiation induced by $\boldsymbol{\sigma_y}$ is much lower than that of radial cracks induced by $\boldsymbol{\sigma_x}$. Besides, it is also found the stress field in the rear of the tip is dominated by the Blister compressive stress. This means that even a median crack was introduced in front of the tip, it might be closed by the compressive stress when the indenter goes through the cracks. Therefore, the tensile stress with low values in front of the indenter and compressive stress in the rear of the indenter jointly reduce the possibility of median crack initiation and propagation, which can be validated by the absence of median cracks in the cross-section FIB-SEM observation in our previous work on the nano scratch of KDP crystal [21].

When it comes to the stress component of $\boldsymbol{\sigma_z}$, the stress distribution is a bit similar to that discussed above. The compressive stress occurs in the area before the indenter while the tensile stress dominates

the residual stress field behind the indenter tip. Meanwhile, the contour line in the area in the rear of the indenter tip is almost parallel to the elastic-to-plastic deformation interface. Considering that this stress component is vertical to the scratch direction, lateral cracks are much easier to be introduced by this tensile stress, as shown in Fig. 6.

Moreover, in order to further understand the temperature effect, the total normal stresses (i.e., the sum of each component) and total shear stress at different temperature with various normal loads are also analyzed and compared, as shown in Fig. 13. One can see that in the area adjacent to the indenter tip, both the normal and shear stress are greatly affected by the temperature. Along the scratching direction (X-axis), the stress field behind the indenter tip is mainly dominated by the tensile stress but its value at AT is higher than that at ET. Given that the Blister stress has been identified as the dominated component in the residual stress field [41], the reduction of tensile tress, as shown in Fig. 13, should be attributed to the decrease of material characteristics (i.e. H, E, ξ) with the rise of temperature, which jointly result in a smaller Blister stress strength at ET comparing with that at RT. Besides, according to the existing analysis, the tensile stress field is generated by the material resistance to the deformation under hydrostatic pressure which is scaled with the applied normal load [7, 45]. Thus, at the same scratch loads (P_n=10mN and 50mN in Fig. 13), the smaller stresses at ET mean a weaker material resistance to deformation, indicating that the material adjacent to the indenter tip at ET is much easier to undergo plastic deformation than that at AT in the scratch process and to be removed with more plastic behaviours (see in Fig. 7). This theoretical analysis result can also be used to explain why the residual indentation morphology at ET shows more plastic features than at RT as shown in Fig. 3.

On the whole, at AT the stress underneath the grooves induced by scratch is very large and increases with the rise of the applied normal load. Once this stress intensity comes close to the material fracture toughness, brittle cracks (e.g., radial cracks, median cracks and lateral cracks) will take place depending on the combination and competition of the stress components; While at ET, the stress underneath the indenter tip induced by scratch is relatively low due to the decreased material hardness, elastic modulus and recovery rate induced by the temperature effect. On the other hand, this temperature effect also simultaneously increases its fracture resistance, as discussed in the nano indentation section. Therefore, the reduced-value stress condition at ET is extremely difficult to approach its fracture toughness, which eventually reduces the risk of crack initiation and hence effectively suppresses crack generation and propagation.

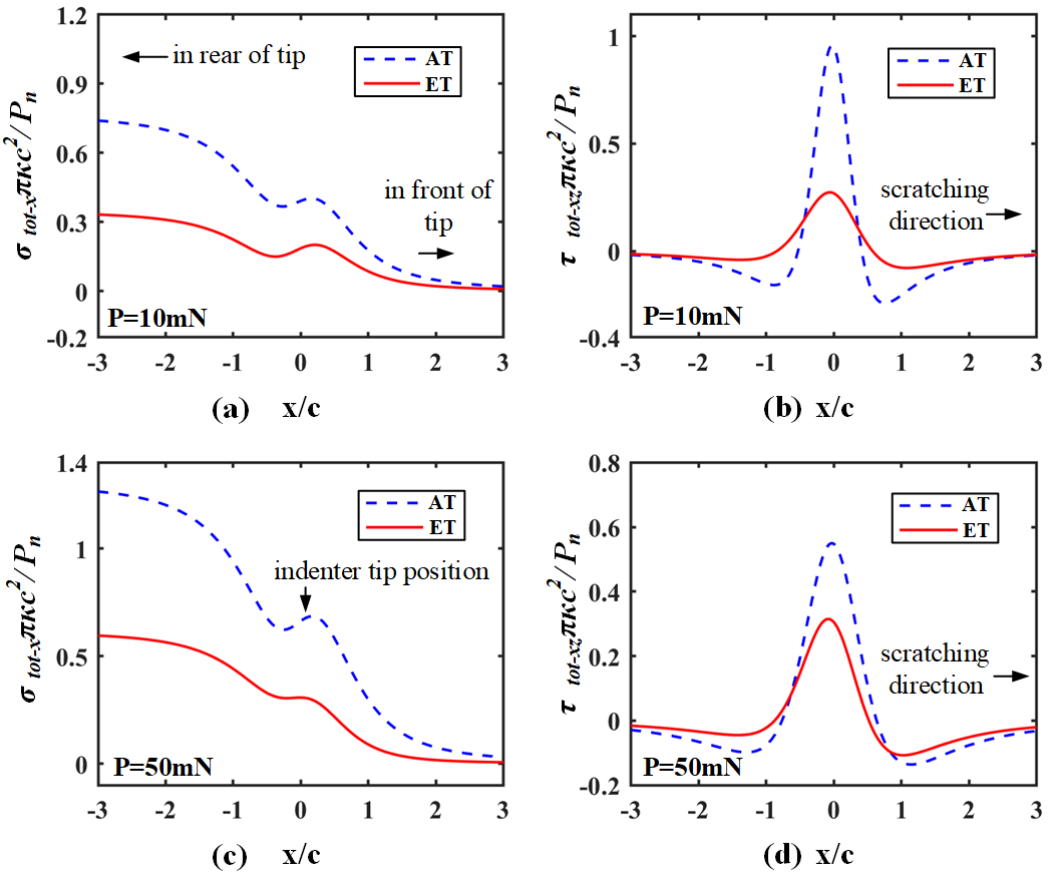

Fig. 13 Comparison of the stress at ambient and elevated temperature along the scratch direction in the XOZ: at the scratch load of P_n=10mN, the total normal stress distribution (a) and total shear stress distribution t (b); at the scratch load of P_n=50mN, the total normal stress distribution (c) and total shear stress (d).

5. Conclusion

In this work, the role of temperature in the ductile removal ability of brittle KDP crystal has been investigated from the perspective of stress analysis and to provide a theoretical explanation for our previous experimental results [21]. Firstly, the specific evolution of material properties induced by temperature change was recalled briefly, followed by varied-depth scratch tests for introducing the different material removal behaviours caused by the temperature effect. Most importantly, an updated stress analytical model has been proposed to explain the underlying evolution mechanism of different brittle features developed at ambient and elevated temperature by considering the change of material properties induced by the temperature effect. It is found that, on the one hand, the fracture resistance of KDP crystal can be enhanced greatly at elevated temperature; while, on the other hand, the tensile stress concentration accumulated in the rear of the indenter tip can be extensively reduced, which is the main reason causing the initiation and propagation of brittle radial and lateral cracks. Thus, as result,

the reduced tensile stress underneath the scratch indenter tip at elevated temperature would become far lower than the improved fracture resistance of KDP crystal, reducing the risk of crack initiation and propagation and eventually improving the ductile-regime removal ability of this type of brittle materials.

Both the experimental result and theoretical analysis all proved that the temperature exerts a positive influence on improving the plastic deformation and ductile removal ability of brittle KDP crystal. These present results about the temperature effect could enlighten the future development of some thermal-involved process in the future and enhance the machinability of brittle materials.

Acknowledgement

This research is supported by the National Natural Science Foundation of China (No. 51775147, 51705105) and Science Challenge Project (No. TZ2016006-0503-01). The authors also appreciate the support from the Nottingham research fellowship programme.

Appendix A

In nano indentation tests with a spherical indenter tip, the hardness can be estimated as the ratio of indentation loads (P_{max}) to the contact area based on the Oliver-Pharr's approach [36]:

$$\begin{cases} H = \dfrac{P_{\max}}{\pi\left(\sqrt{2Rh_c - h_c^2}\right)^2} \\ h_c = h_{max} - \varepsilon \dfrac{P_{\max}}{S} \end{cases} \tag{A.1}$$

where R and h_c account for the radius of the indenter tip and contact depth, respectively; ε=0.75 is suggested for spherical indenters. S donates slopes of unloading curves and can be given by $S = dP/dh$.

Meanwhile, the Elastic Modulus, E, can be expressed as [36]:

$$\begin{cases} E_s = \left(1 - v_s^2\right) \Big/ \left(\dfrac{1}{E_r} - \dfrac{1 - v_i^2}{E_i}\right) \\ E_r = S \Big/ \left(2\sqrt{2Rh_c - h_c^2}\right) \end{cases} \tag{A.2}$$

where v_s and E_s represent the Poisson's ratio and Elastic modulus of indenters; v_i and E_i indicate the same meaning for samples. By refering to the existing research, the E_i and v_i for diamond indenters can be set as 1141 GPa and 0.07.

Furthermore, according to the indentation fracture theory, the spherical indentation fracture toughness can be estimated as [48]:

$$K_{IC} = \xi(\frac{E}{H})^{1-m}(\frac{\pi}{12})^{2/3}\left[3\tan\frac{\varphi}{2} + (\tan\frac{\varphi}{2})^2\right]^{2/3}\frac{P_{\max}}{c^{3/2}} \quad (A.3)$$

Where the terms m and ξ are dimensionless constant and can be given as 0.5 and 0.032 in spherical indentations [21]; c is the crack length; φ could be given by $\arcsin(a/R)$ while a is the radius of indentation contact circles.

Appendix B

The Boussinesq stress field is given as:

$$\sigma_x^n = \frac{P_n}{2\pi c^2}\left[\frac{1-2\nu}{r^2}\left\{(1-\frac{z}{\rho})\frac{x^2-y^2}{r^2} + \frac{z*y^2}{\rho^3}\right\} - \frac{3*z*x^2}{\rho^5}\right] \quad (B.1)$$

$$\sigma_y^n = \frac{P_n}{2\pi c^2}\left[\frac{1-2\nu}{r^2}\left\{(1-\frac{z}{\rho})\frac{y^2-x^2}{r^2} + \frac{z*x^2}{\rho^3}\right\} - \frac{3*z*x^2}{\rho^5}\right] \quad (B.2)$$

$$\sigma_z^n = -\frac{3P_n}{2\pi c^2}\frac{z^3}{\rho^5} \quad (B.3)$$

$$\tau_{xy}^n = \frac{P_n}{2\pi c^2}\left[\frac{1-2\nu}{r^2}\left\{(1-\frac{z}{\rho})\frac{x*y}{r^2} - \frac{x*y*z}{\rho^3}\right\} - \frac{x*y*z}{\rho^5}\right] \quad (B.4)$$

$$\tau_{yz}^n = \frac{3P_n}{2\pi c^2}\frac{y*z^z}{\rho^5} \quad (B.5)$$

$$\tau_{yz}^n = \frac{3P_n}{2\pi c^2}\frac{x*z^z}{\rho^5} \quad (B.6)$$

The Cerruti stress field is given as:

$$\sigma_x^t = -\frac{P_t}{2\pi c^2}\left[\frac{3x^3}{\rho^5} - (1-2\nu)\left\{\frac{x}{\rho^3} - \frac{3x}{\rho(\rho+z)^2} + \frac{x^3}{\rho^3(\rho+z)^2} + \frac{2x^3}{\rho^2(\rho+z)^3}\right\}\right] \quad (B.7)$$

$$\sigma_y^t = -\frac{P_t}{2\pi c^2}\left[\frac{3x*y^2}{\rho^5} - (1-2\nu)\left\{\frac{x}{\rho^3} - \frac{x}{\rho(\rho+z)^2} + \frac{x*y^2}{\rho^3(\rho+z)^2} + \frac{2x*y^2}{\rho^2(\rho+z)^3}\right\}\right] \quad (B.8)$$

$$\sigma_z^t = -\frac{3P_t}{2\pi c^2}\frac{x*z^2}{\rho^5} \quad (B.9)$$

$$\tau_{xy}^{t}=-\frac{P_t}{2\pi c^2}\left[\frac{3x^2*y}{\rho^5}+(1-2\nu)\left\{\frac{y}{\rho(\rho+z)^2}+\frac{x^2*y}{\rho^3(\rho+z)^2}-\frac{2x^2*y}{\rho^2(\rho+z)^3}\right\}\right] \quad \text{(B.10)}$$

$$\tau_{yz}^{t}=-\frac{3P_t}{2\pi c^2}\frac{x*y*z}{\rho^5} \quad \text{(B.11)}$$

$$\tau_{yz}^{t}=-\frac{3P_t}{2\pi c^2}\frac{x^2*y*z}{\rho^5} \quad \text{(B.12)}$$

The Blister residual stress field is expressed as follows:

$$\begin{aligned}\sigma_x^r=\frac{2B}{(y^2+z^2)^2c^2}\Big\{&-2\nu(y^2-z^2)+\frac{x}{\rho^5}(2\nu x^4y^2-2x^2y^4+6\nu x^2y^4\\&-2y^6+4\nu y^6-2\nu x^4z^2-4x^2y^2z^2+2\nu x^2y^2z^2-3y^4z^2+6\nu y^4z^2\\&-2x^2z^4-4\nu x^2z^4+z^6-2\nu z^6)\Big\}\end{aligned} \quad \text{(B.13)}$$

$$\begin{aligned}\sigma_y^r=\frac{2B}{(y^2+z^2)^3c^2}\Big\{&-2y^2(y^2-3z^2)+\frac{x}{\rho^5}(2\nu x^4y^4-2\nu x^2y^6+6x^2y^6\\&+4y^8-2\nu y^8-6x^4y^2z^2-7x^2y^4z^2-6\nu x^2y^4z^2-2y^6z^2-8\nu y^6z^2-12x^2y^2z^4\\&-6\nu x^2y^2z^4-15y^4z^4-12\nu y^4z^4+x^2z^6-2\nu x^2z^6-8y^2z^6+z^8-2\nu z^8)\Big\}\end{aligned} \quad \text{(B.14)}$$

$$\begin{aligned}\sigma_z^r=\frac{2Bz^2}{(y^2+z^2)^3c^2}\Big\{&2(z^2-3y^2)+\frac{x}{\rho^5}(10x^2y^2z^2+12y^4z^2+9y^6-2x^4z^2\\&-5x^2z^4+6x^4y^2+15x^2y^4-3y^2z^4-6z^6)\Big\}\end{aligned} \quad \text{(B.15)}$$

$$\tau_{xy}^r=\frac{2By}{\rho^5c^2}\left\{2(1-\nu)x^2+2(1-\nu)y^2-z^2-2\nu z^2)\right\} \quad \text{(B.16)}$$

$$\begin{aligned}\tau_{yz}^r=-\frac{2By*z}{(y^2+z^2)^2c^2}\Bigg[&\frac{4\left(y^2-x^2\right)}{y^2+z^2}-\frac{x}{\rho^5}\left\{4x^4y^2+10x^2y^4+6y^6-4x^4z^2\right.\\&\left.-12y^2z^4-9z^6+3y^4z^2-10x^2z^4)\right\}\end{aligned} \quad \text{(B.17)}$$

$$\tau_{zx}^r=\frac{2Bz}{\rho^5c^2}\left\{2x^2+2y^2-z^2\right\} \quad \text{(B.18)}$$

Reference

[1] Q. Liu, J. Cheng, Z. Liao, H. Yang, L. Zhao, M. Chen, Incident laser modulation by tool marks on micro-milled KDP crystal surface: Numerical simulation and experimental verification, Optics & Laser Technology, 119 (2019) 105610.

[2] S. Yang, L. Zhang, Characterization of mechanical properties and failure of potassium dihydrogen phosphate under mechanical stressing, Ceramics International, (2021).

[3] Q. Liu, Z. Liao, J. Cheng, D. Xu, M. Chen, Mechanism of chip formation and surface-defects in orthogonal cutting of soft-brittle potassium dihydrogen phosphate crystals, Materials & Design, 198 (2021).

[4] H. Yang, J. Cheng, Z. Liu, Q. Liu, L. Zhao, C. Tan, J. Wang, M. Chen, Potential damage threats to downstream optics caused by Gaussian mitigation pits on rear KDP surface, High Power Laser Science and Engineering, 8 (2020) 37-31.

[5] Q. Liu, J. Cheng, Y. Xiao, H. Yang, M. Chen, Effect of milling modes on surface integrity of KDP crystal processed by micro ball-end milling, Procedia CIRP, 71 (2018) 260-266.

[6] N. Chen, L. Li, J. Wu, J. Qian, N. He, D. Reynaerts, Research on the ploughing force in micro milling of soft-brittle crystals, International Journal of Mechanical Sciences, 155 (2019) 315-322.

[7] C. Li, Y. Zhang, G. Zhou, Z. Wei, L. Zhang, Theoretical modelling of brittle-to-ductile transition load of KDP crystals on (001) plane during nanoindentation and nanoscratch tests, Journal of Materials Research and Technology, 9 (2020) 14142-14157.

[8] S. Yang, L. Zhang, Z. Wu, Characterization and criteria of phase transformations and lattice slipping in potassium dihydrogen phosphate crystals, Journal of the American Ceramic Society, (2021).

[9] N. Chen, M. Chen, C. Wu, X. Pei, J. Qian, D. Reynaerts, Research in minimum undeformed chip thickness and size effect in micro end-milling of potassium dihydrogen phosphate crystal, International Journal of Mechanical Sciences, 134 (2017) 387-398.

[10] B. Meng, D. Yuan, S. Xu, Study on strain rate and heat effect on the removal mechanism of SiC during nano-scratching process by molecular dynamics simulation, International Journal of Mechanical Sciences, 151 (2019) 724-732.

[11] D. Xu, Z. Liao, D. Axinte, M. Hardy, A novel method to continuously map the surface integrity and cutting mechanism transition in various cutting conditions, International Journal of Machine Tools and Manufacture, 151 (2020).

[12] Y.J. Lee, A.S. Kumar, H. Wang, Beneficial stress of a coating on ductile-mode cutting of single-crystal brittle material, International Journal of Machine Tools and Manufacture, (2021) 103787.

[13] Z. Liao, A. Abdelhafeez, H. Li, Y. Yang, O.G. Diaz, D. Axinte, State-of-the-art of surface integrity in machining of metal matrix composites, International Journal of Machine Tools and Manufacture, 143 (2019) 63-91.

[14] X. Rao, F. Zhang, X. Luo, F. Ding, Y. Cai, J. Sun, H. Liu, Material removal mode and friction behaviour of RB-SiC ceramics during scratching at elevated temperatures, Journal of the European Ceramic Society, (2019).

[15] K. You, G. Yan, X. Luo, M.D. Gilchrist, F. Fang, Advances in laser assisted machining of hard and brittle materials, Journal of Manufacturing Processes, 58 (2020) 677-692.

[16] J. Feng, Z. Wan, W. Wang, X. Huang, X. Ding, Y. Tang, Unique crack behaviors of glass BK7 occurred in successive double scratch under critical load of median crack initiation, Journal of the European Ceramic Society, 40 (2020) 3279-3290.

[17] W. Huang, J. Yan, Chip-free surface patterning of toxic brittle polycrystalline materials through micro/nanoscale burnishing, International Journal of Machine Tools and Manufacture, 162 (2021).

[18] C.H. Guin, M.D. Katrich, A.I. Savinkov, M.P. Shaskolskaya, Plastic strain and dislocation structure of the KDP group crystals, Kristall und Technik, 15 (1980) 479-488.

[19] J. Borc, K. Sangwal, I. Pritula, E. Dolzhenkova, Investigation of pop-in events and indentation size effect on the (001) and (100) faces of KDP crystals by nanoindentation deformation, Materials Science and Engineering: A, 708 (2017) 1-10.

[20] C. Li, X. Li, Y. Wu, F. Zhang, H. Huang, Deformation mechanism and force modelling of the grinding of YAG single crystals, International Journal of Machine Tools and Manufacture, 143 (2019) 23-37.

[21] Q. Liu, Z. Liao, D. Axinte, Temperature effect on the material removal mechanism of soft-brittle crystals at nano/micron scale, International Journal of Machine Tools and Manufacture, 159 (2020) 103620.

[22] S. Yang, L. Zhang, H. Xie, W. Liu, Interaction potential function for the deformation analysis of potassium dihydrogen phosphate using molecular dynamics simulation, Computational Materials Science, 187 (2021).

[23] P. Huang, S. Wang, J. Ding, D. Wang, H. Liu, L. Xu, X. Li, G. Liu, B. Wang, Study on fracture toughness of potassium dihydrogen phosphate single crystal, CrystEngComm, (2019).

[24] J. Feng, Z. Wan, W. Wang, X. Huang, X. Ding, Z. Jiang, Scratch with double-tip tool: Crack behavior during simultaneous double scratch on BK7 glass, Journal of the European Ceramic Society, 40 (2020) 4202-4216.

[25] M. Li, X. Guo, R. Zhai, X. Luo, R. Kang, Z. Jin, D. Guo, Study on the subsurface damage mechanism of optical quartz glass during single grain scratching, Ceramics International, 47 (2021) 7683-7691.

[26] S. Yang, L. Zhang, Z. Wu, An investigation on the nano-abrasion wear mechanisms of KDP crystals, Wear, 476 (2021).

[27] X. Rao, F. Zhang, Y. Lu, X. Luo, F. Chen, Surface and subsurface damage of reaction-bonded silicon carbide induced by electrical discharge diamond grinding, International Journal of Machine Tools and Manufacture, 154 (2020).

[28] C. Li, F. Zhang, X. Wang, X. Rao, Investigation on surface/subsurface deformation mechanism and mechanical properties of GGG single crystal induced by nanoindentation, Appl Opt, 57 (2018) 3661-3668.

[29] E.H. Yoffe, Elastic stress fields caused by indenting brittle materials, Philosophical Magazine A, 46 (2006) 617-628.

[30] Y. Ahn, T.N. Farris, S. Chandrasekar, Sliding microindentation fracture of brittle materials: Role of elastic stress fields, Mechanics of Materials, 29 (1998) 143-152.

[31] Q. Liu, J. Cheng, Y. Xiao, M. Chen, H. Yang, J. Wang, Effect of tool inclination on surface quality of KDP crystal processed by micro ball-end milling, The International Journal of Advanced Manufacturing Technology, 99 (2018) 2777-2788.

[32] Q. Liu, J. Cheng, H. Yang, Y. Xu, L. Zhao, C. Tan, M. Chen, Modeling of residual tool mark formation and its influence on the optical performance of KH2PO4 optics repaired by micro-milling, Opt. Mater. Express, 9 (2019) 3789.

[33] L. Anand, N. Ames, On modeling the micro-indentation response of an amorphous polymer, International Journal of Plasticity, 22 (2006) 1123-1170.

[34] X. Guo, X. Zhang, X. Tang, D. Guo, H. Gao, X. Teng, Nanoindentation on the doubler plane of KDP single crystal, Journal of Semiconductors, 34 (2013).

[35] Z. Liao, A. la Monaca, J. Murray, A. Speidel, D. Ushmaev, A. Clare, D. Axinte, R. M'Saoubi, Surface integrity in metal machining - Part I: Fundamentals of surface characteristics and formation mechanisms, International Journal of Machine Tools and Manufacture, 162 (2021).

[36] W.C. Oliver, G.M. Pharr, Measurement of hardness and elastic modulus by instrumented indentation: Advances in understanding and refinements to methodology, Journal of Materials Research, 19 (2004) 3-20.

[37] B.R. Lawn, Indentation of Ceramics with Spheres: A Century after Hertz, Journal of the American Ceramic Society, 81 (1998) 1977-1994.

[38] T. Fang, J.C. Lambropoulos, Microhardness and Indentation Fracture of Potassium Dihydrogen Phosphate (KDP), Journal of the American Ceramic Society, 85 (2004) 174-178.

[39] S.O. Kucheyev, W.J. Siekhaus, T.A. Land, S.G. Demos, Mechanical response of KD2xH2(1−x)PO4 crystals during nanoindentation, Applied Physics Letters, 84 (2004) 2274-2276.

[40] Q. Jiang, L. Zhang, C. Yang, Research on material removal mechanism and radial cracks during scribing single crystal gallium nitride, Ceramics International, (2021).

[41] W. Wang, P. Yao, J. Wang, C. Huang, T. Kuriyagawa, H. Zhu, B. Zou, H. Liu, Elastic stress field model and micro-crack evolution for isotropic brittle materials during single grit scratching, Ceramics International, 43 (2017) 10726-10736.

[42] X. Jing, S. Maiti, G. Subhash, A New Analytical Model for Estimation of Scratch-Induced Damage in Brittle Solids, Journal of the American Ceramic Society, 90 (2007) 885-892.

[43] S. Lafaye, C. Gauthier, R. Schirrer, The ploughing friction: analytical model with elastic recovery for a conical tip with a blunted spherical extremity, Tribology Letters, 21 (2006) 95-99.

[44] C. Li, F. Zhang, Y. Wu, X. Zhang, Influence of strain rate effect on material removal and deformation mechanism based on ductile nanoscratch tests of Lu2O3 single crystal, Ceramics International, 44 (2018) 21486-21498.

[45] L. Huang, C. Bonifacio, D. Song, K.v. Benthem, A.K. Mukherjee, J.M. Schoenung, Investigation into the microstructure evolution caused by nanoscratch-induced room temperature deformation in M-plane sapphire, Acta Materialia, 59 (2011) 5181-5193.

[46] B.R. Lawn, D.B. Marshall, Indentation Fractography: A Measure of Brittleness, Journal of Research of the National Bureau of Standards, 89 (1984) 435-451.

[47] X. Gu, Q. Zhao, H. Wang, J. Xue, B. Guo, Fundamental study on damage-free machining of sapphire: Revealing damage mechanisms via combining elastic stress fields and crystallographic structure, Ceramics International, 45 (2019) 20684-20696.

[48] Z. Chen, X. Wang, A. Atkinson, N. Brandon, Spherical indentation of porous ceramics: Elasticity and hardness, Journal of the European Ceramic Society, 36 (2016) 1435-1445.